POLITECNICO DI TORINO
Repository ISTITUZIONALE

Analysis of Hydrodynamic-Induced Stress in the Bossea Mountain Karst Aquifer through Passive Seismic Monitoring

Original
Analysis of Hydrodynamic-Induced Stress in the Bossea Mountain Karst Aquifer through Passive Seismic Monitoring / Biamino, L., Colombero, C., Vagnon, F., Fiorucci, A., Vigna, B.. - ELETTRONICO. - (2026). (IAEG 2026: Engineering Geology in a Rapidly Changing World - XV IAEG World Congress Delft (Nld) 30 October - 6 November 2026) [10.59490/6ad293c76ee698573e4dd1a1].

Availability:
This version is available at: 11583/3017244 since: 2026-10-30T16:18:53Z

Publisher:
TU Delft OPEN Publishing

Published
DOI:10.59490/6ad293c76ee698573e4dd1a1

Terms of use:

This article is made available under terms and conditions as specified in the corresponding bibliographic description in the repository

Publisher copyright

(Article begins on next page)

10 November 2026

DOI: 10.59490/6ad293c76ee698573e4dd1a1

TU Delft | OPEN Publishing

Proceedings of the 15th IAEG World Congress IAEG 2026
Engineering Geology in a Rapidly Changing World
30 October to 6 November 2026
Delft University of Technology, The Netherlands

Analysis of Hydrodynamic-Induced Stress in the Bossea Mountain Karst Aquifer through Passive Seismic Monitoring

Luca Biamino[1,*], Chiara Colombero[1], Federico Vagnon[1], Adriano Fiorucci[1], and Bartolomeo Vigna[1,2]

[1]Department of Environment, Land and Infrastructure Engineering (DIATI), Politecnico di Torino, C.so Duca degli Abruzzi 24, 10129, Torino, Italy; luca.biamino@polito.it, https://orcid.org/0009-0009-9990-9794; chiara.colombero@polito.it, https://orcid.org/0000-0001-9818-7464; federico.vagnon@polito.it, https://orcid.org/0000-0003-0539-0557; adriano.fiorucci@polito.it, https://orcid.org/0000-0002-6909-2121; bartolomeo.vigna@formerfaculty.polito.it, https://orcid.org/0000-0003-2272-8740

[2] Bossea Underground Karst Laboratory, Club Alpino Italiano, Cuneo, Italy

*corresponding author

ABSTRACT

Continuous passive seismic monitoring has provided insights into detecting and tracking the evolution of the rock mass responses under hydro-mechanical processes at multi-daily timescales. The *Bossea* Cave is a mountain karst aquifer located in the Ligurian Alps (Piedmont, NW Italy). It developed at the contact between a Permian impermeable meta-volcanic basement and an overlying Triassic meta-carbonate sequence. This upper unit controls the drainage of infiltrating water, mainly driven by rainfall and snowmelt processes occurring in the aquifer's recharge area. The seismic signature of these water inflows was investigated using a three-component seismometer installed in the hypogeal environment. Ambient-noise Power Spectral Density (PSD) was computed on each component to identify high-energy frequency bands and examine their temporal evolution, comparing it with the discharge trends of the main drain (*Mora* Creek). A strong correlation was detected at approximately 33 Hz on the North, East, and vertical components, with a zero-lag response under ordinary recharge conditions. In contrast, during extreme inflow events (e.g., October 2020), increases in seismic-noise amplitude preceded the discharge peak by approximately 4 hours. These observations complement the results of a temporary external seismometer survey deployed on the slope above the cave in 2022, where precipitation-driven modulation was identified in the 50–90 Hz band and a 30-Hz amplification occurred about 4 hours before the peak discharge. This combined evidence provides a basis for investigating the triggering mechanisms of coupled thermo- and hydro-induced rock-mass deformation and for characterizing the spectral signatures of impulsive microseismic signals potentially associated with incipient fracturing.

KEYWORDS: karst aquifer, passive seismic methods, hydrodynamics, spectral analysis.

INTRODUCTION

The *Bossea* cave is a dead-end hypogeal site in the *Corsaglia* valley (SW Piedmont, Figure 1a), extending for approximately 3 km from the access conduit at 836 m a.s.l. to the terminal sumps at 964 m a.s.l. in elevation. The cave developed along the contact between Permian volcanoclastic rocks, resting on a deeply buried Variscan basement, and an overlying, partially detached Meso-Cenozoic sedimentary sequence, within the *Internal Ligurian Briançonnais* domain that marks the transition between the Western Ligurian and the Maritime Alps (Antonellini et al., 2019). This area hosts several carbonate aquifers characterized by extensive vadose zones and high-elevation recharge areas, reflecting tectonic uplift associated with Alpine orogenesis. Aquifer recharge is tightly controlled by the Alpine regional climate, with winter inputs dominated by solid precipitation (Vigna & Banzato, 2015). Snowmelt typically begins when the snowpack becomes isothermal at 0 °C, generally from April onward, generating pronounced recharge pulses and potentially severe floods when superimposed on spring rainfall. Summer recharge is mainly limited to scattered convective storms, whereas early autumn is often characterized by intense precipitations capable of producing exceptional high-flow floods (Nannoni et al., 2020; Vigna & Banzato, 2015). Consistent with the broader Western Alps, the area is increasingly

Published: 30/10/2026
©2026 published by TU Delft OPEN Publishing on behalf of the authors under CC-BY-4.0 license

DOI: 10.59490/6ad293c76ee698573e4dd1a1

affected by climate change, with enhanced advection of warm air masses from the Mediterranean basin and a progressive shift toward a higher fraction of autumn precipitation falling as rain rather than snow (Bozzoli et al., 2024).

The recharge area of the *Bossea* aquifer extends between 800 and 1700 m a.s.l. and is characterised by both autogenic inputs, i.e. rainfall and snowmelt infiltrating into Middle Triassic–Cretaceous limestones and dolomitic limestones, and allogenic inputs, namely the capture of surface runoff through sinkholes developed along detachment surfaces above impermeable pre-Triassic formations (Antonellini et al., 2019; Nannoni et al., 2020). Accordingly, discharge at the main drain (named *Mora* Creek) is strongly modulated by seasonal recharge and ranges from a baseflow of 0.060 $m^3 s^{-1}$ to exceptional peak values (e.g. 1.14 $m^3 s^{-1}$ on 3 October 2020, following 293 mm of rainfall on 2 October 2020, Biamino et al., 2024). The main drain generally exhibits a rapid hydrodynamic response to recharge events; however, exceptional floods that activate a broader portion of the catchment area promote substantial remobilization of long-residence-time water, whereas this additional contribution is less pronounced during snowmelt-driven infiltration (Nannoni et al., 2020). These dynamics are supported by geochemical evidence, including variations in dissolved radon (Rn), electrical conductivity, transport of fine mineral-rich suspended particles, and rare earth element (REE) signatures (Biamino et al., 2024; Fiorucci et al., 2015; Nannoni et al., 2020). Furthermore, *Mora* Creek provides the primary hydrodynamic forcing on speleogenesis and thus controls the morphostructural evolution of the cave (Antonellini et al., 2019). The system is subdivided into two main sectors (Figure 1b): the upper segment, where the cave develops predominantly sub-horizontally within the Mesozoic marbles through carbonate dissolution, including several perched phreatic conduits; and the lower segment, characterized by large collapse structures developed near the contact between the marbles and the underlying impermeable metavolcanics. In the latter sector, mechanical erosion and gravitational processes prevail, promoting roof instabilities involving meta-carbonate duplex structures (Antonellini et al., 2019). This area is also accessible to tourists and hosts an underground karst laboratory for multidisciplinary research jointly operated by the Politecnico di Torino and the Scientific Committee of the Italian Alpine Club.

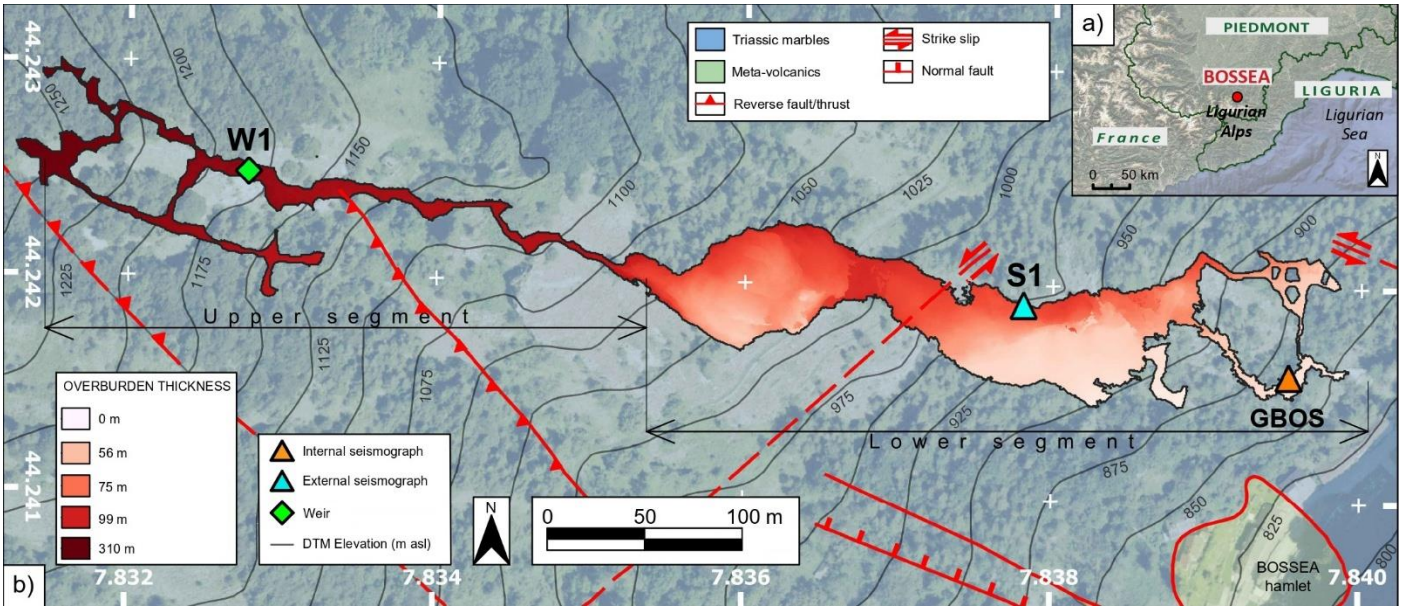


Figure 1. **a)** Location of the investigated site. **b)** Planimetric view showing outcropping rock formations and the subdivision of the *Bossea* cave into the lower (touristic) and the upper sectors. Overburden thickness was computed as the difference between the external Digital Terrain Model and the cave-vault Digital Elevation Model, and subsequently rasterized. The internal (GBOS) and external (S1) seismographs are indicated, as well as the *Mora* Creek discharge monitoring point (W1). Reference system: WGS 84 geographic coordinates (EPSG:4326). Basemaps: *Geological Map of the Piedmont Region* (1:250,000; ARPA Piemonte CNR-IGG) and *2024 AGEA Regional Orthophoto* (Regione Piemonte).

Temporal variability in the aquifer recharge and discharge imposes hydraulic-head transients within the fracture-conduit network, resulting in a time-dependent hydraulic load on the surrounding rock mass and effective-stress perturbations along discontinuities (Almagro Vidal et al., 2021). Recent failures affecting sub-vertical discontinuity sets have been documented near the cave boundary at the impermeable basement–marble contact, suggesting a cyclic loading regime in which repeated hydraulic transients promote damage accumulation and episodic rupture through time-varying normal stress and shear resistance. In this context, ambient-noise

DOI: 10.59490/6ad293c76ee698573e4dd1a1

seismology has been successfully applied to relate temporal variations in noise amplitude and seismic velocity to changes in water storage, hydraulic gradients, and flow regime within fracture-conduit networks (Almagro Vidal et al., 2021; Fores et al., 2018; Pantiga et al., 2025). Accordingly, the hydromechanical forcing associated with transient groundwater inflow was investigated through passive seismic monitoring during different periods: October 2020, April-March 2021, and May 2022. The latter was specifically selected to enable a joint interpretation of subsurface and surface seismic observations by comparing the internal sensor installed within the access conduit with an external station placed on the slope above the cave. This comparison extended earlier findings that highlighted a strong precipitation-driven modulation of seismic noise energy in the 50-90 Hz band (Dabove et al., 2023). Power spectral density (PSD) estimates were computed to isolate high-energy frequency bands exhibiting systematic sensitivity to hydraulic loading. Internal-external comparisons of the spectral signatures were therefore used to improve source attribution and to discriminate subsurface, flow-related contributions from surface and near-surface processes (i.e., rainfall impact, runoff), refining the interpretation of the observed noise field.

METHODS

Meteorological variables were continuously monitored at the *Borello* station (970 m a.s.l.), operated by the Regional Environmental Protection Agency of Piedmont (*ARPA Piemonte - Agenzia Regionale per la Protezione Ambientale*) and located 2 km from the *Bossea* cave. Precipitation was measured using an unheated *PMB2/R-CAE* tipping-bucket rain gauge (resolution 10^{-1} mm) and recorded at 10 min intervals, while air temperature was recorded every 30 min with 10^{-1} °C resolution. The hydrometric level of the *Mora* Creek in the aquifer was recorded at 15-minute intervals with millimetre-level resolution (10^{-3} m) at a gauging weir (W1, Figure 1b) in the upper-canyon segment of the cave and subsequently converted to discharge values Q [$m^3 s^{-1}$] using the Equation (1) given for a Bazin rectangular weir:

$$Q = 0.385 \cdot bh_0 \cdot \sqrt{2gh_0} \quad (1)$$

where h_0 [m] denotes the hydraulic head over the crest, b [m] the constant weir width (1.2 m) and g the gravity [$m\ s^{-2}$].

Seismic activity inside the cave was monitored using a *Nanometrics Trillium 240 s* seismometer coupled to *a Nanometrics Taurus* recorder. The instrument was installed in a small, confined cavity beside the entrance conduit (Figure 1b), where the overburden thickness is limited (26 m). Continuous three-component seismic data (HHE, HHN, and HHZ, where the first H denotes a high-sampling-rate band, the second H denotes a high-gain channel, and E, N, and Z indicate the East-West, North-South, and vertical components of ground motion, respectively) were sampled at 100 Hz and retrieved from the European Integrated Data Archive (EIDA) through the Italian node for network GU (University of Genoa, 1967), station GBOS. Waveforms were pre-processed using the open-source *ObsPy* Python toolbox (Krischer et al., 2015 - version 4.1.2), including instrument-response removal to convert raw counts to ground velocity ($m\ s^{-1}$). Prior to spectral analysis, records were demeaned and band-pass filtered (1–48 Hz; Butterworth type). To mitigate the influence of transient energetic signals on noise spectra, amplitude clipping was applied using an adaptive threshold set to ±4 standard deviations of the pre-processed waveform (Bendat & Piersol, 2010; McNamara & Buland, 2004). Hourly Power Spectral Density (PSD) estimates were computed using a Welch-type procedure (Welch, 1967). Each 1-h record was partitioned into consecutive, non-overlapping 100-s segments and tapered with a 10% cosine window. PSDs were computed for each segment, corrected for taper-induced amplitude loss, and finally averaged to obtain a representative hourly PSD with reduced variance. High-energy frequency bands were accurately selected from the PSD time series and the corresponding band-limited amplitude metrics (measured in [$m^2\ s^{-2}\ Hz^{-1}$]) were extrapolated as proxies for the identification of the rock-mass seismic signature. The resulting time series were then low-pass filtered using a 12-hour cutoff period to mitigate Butterworth edge distortion over each one-day segment. Finally, for each monitored interval (Table 1), the filtered three-component seismic time series were component-averaged and cross-correlated with the *Mora* Creek discharge to estimate the seismic–discharge lag. Additionally, the discharge time series was cross-correlated with the meteorological variables to estimate the delay between rainfall (or atmospheric temperature in case of snowmelt) and the resulting discharge signal at the weir (W1). The resulting lag estimates were combined to constrain the relative timing among seismic energy variations, transient hydraulic loading, and atmospheric forcing. During the 5–15 May 2022 interval, the concurrent operation of the internal seismometer (GBOS) and external station (S1, *Nanometrics Trillium 20 s* coupled to a *Nanometrics Pegasus* recorder and installed a few tens of centimetres below the ground surface on the slope at the top of the cave, Dabove et al., 2023), also enabled a specifical double depth-dependent comparison of the seismic response.

RESULTS AND DISCUSSION

The temporal evolution of ambient-noise power spectral densities was evaluated under three representative hydrological forcing conditions: an extreme rainfall-driven flood (October 2020), a snowmelt-driven discharge increase (March-April 2021), and an ordinary spring rainfall-driven flood, captured simultaneously by the internal (GBOS) and external (S1) stations (May 2022). These

DOI: 10.59490/6ad293c76ee698573e4dd1a1

cases span impulsive to gradual recharge, enabling the relative contributions of hydraulic loading and atmospheric forcing to be distinguished in the recorded seismic signature.

Table 1. Cross-correlation results. For each analysed interval, the lag and the corresponding maximum cross-correlation value ρ_{xy} are indicated.

Interval	***GBOS-Q***	***S1-Q***	***Q-RF***	***Q-T***
1-6 October 2020	*lag: -4 h*	-	*lag: +8 h*	-
Rainfall	*ρ_{xy}: 0.96*		*ρ_{xy}: 0.87*	
20 March – 7 April 2021	*lag: 0 h*	-	-	*lag: +9 h*
Snowmelting	*ρ_{xy}: 0.98*			*ρ_{xy}: 0.75*
5 – 15 May 2022	*lag: 0 h*	*lag: -4 h*	*lag: +10 h*	-
Rainfall	*ρ_{xy}: 0.97*	*ρ_{xy}: 0.89*	*ρ_{xy}: 0.66*	

Extreme rainfall event: 2–3 October 2020

An extreme hydrological response was recorded on 3 October 2020, with a peak discharge of 1.14 $m^3 s^{-1}$, following 293 mm of rainfall on 2 October 2020 (Figure 2a). The seismic response exhibited high energy levels, with amplitudes on the horizontal components (East and North, Figure 2b and Figure 2c, respectively) exceeding those on the vertical component (Figure 2d). Although the strongest amplification coincided with a broadband energy increase, spectral amplification was most evident in the 33-Hz band (maximum amplitude of -120 dB), providing a robust marker of the event-related response (Figure 2e). A secondary, weaker amplification was also observed near 12 Hz, consistent with previous case studies (Fores et al., 2018; Pantiga et al., 2025). However, this feature was largely confined to the event peak and diminished rapidly thereafter. Indeed, the predominance of the 33-Hz amplification may reflect the regime acting within the aquifer's main drain, potentially shifting the seismic signature toward higher frequencies during sustained turbulent high-flow conditions. Cross-correlation further indicates that the PSD signal led discharge by 4 hours (negative lag relative to discharge, $\rho_{xy} = 0.96$) and lagged rainfall by 4 hours (positive lag relative to rainfall, $\rho_{xy} = 0.87$), as detailed in Figure 2f and Table 1. This timing supports a process-based interpretation, in which the early flood phase appears to be controlled by rapid infiltration and piston-flow dynamics (Nannoni et al., 2020). In this framework, incoming water volumes mobilize long-resident groundwater and induce a mechanical stress perturbation that propagates through the fractured rock mass faster than the hydraulic pressure signal governing the discharge peak of the main drain. The predominance of horizontal motion is consistent with this interpretation, suggesting a stronger sensitivity of the E–N components to event-related stress redistribution. Finally, the 12-h filtered seismic time series shows a near absence of sub-daily periodicity, indicating that event-scale hydrodynamics fully dominates the seismic response and masks any potential atmospheric thermal forcing.

DOI: 10.59490/6ad293c76ee698573e4dd1a1

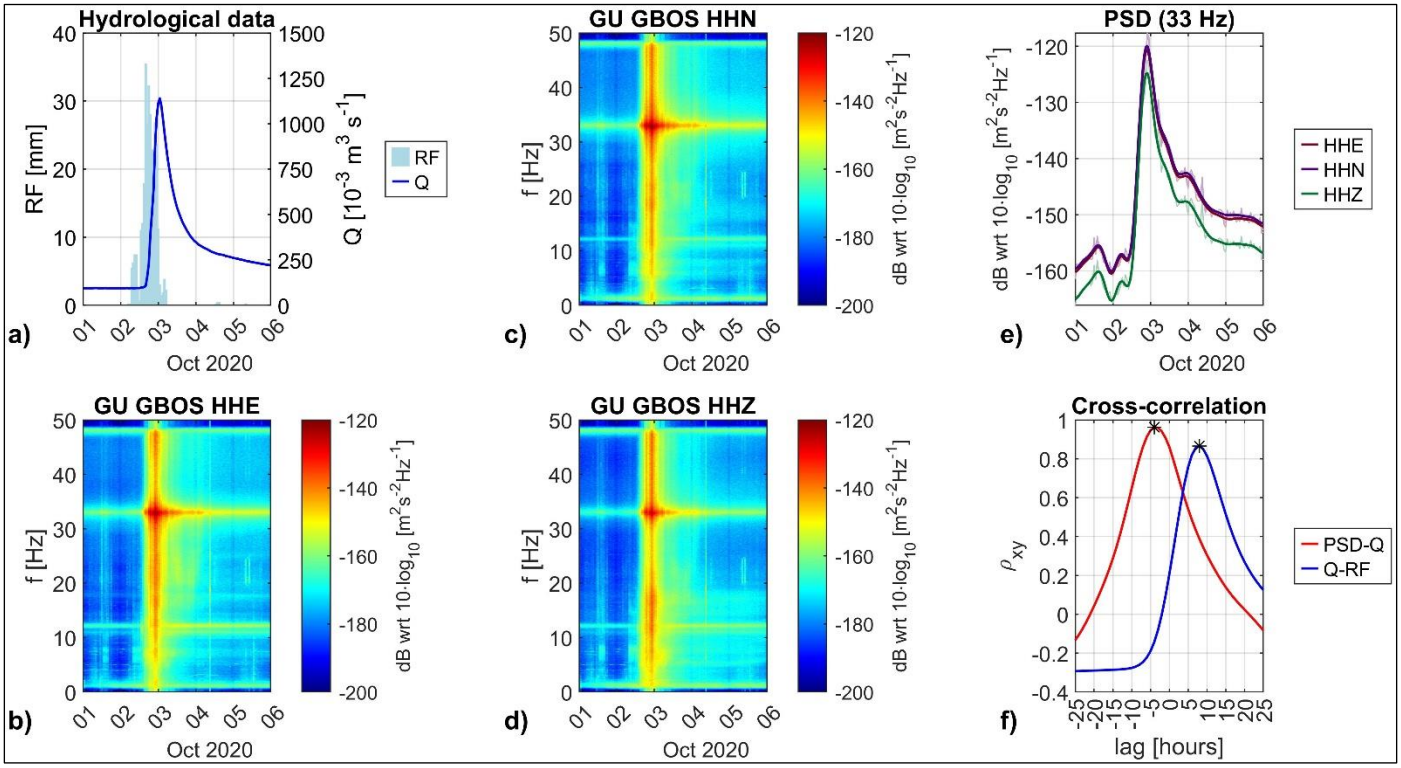


Figure 2. Power spectral densities (PSD) of seismic recordings from 1 to 6 October 2020, including an extreme rainfall–flood event. **a)** Discharge (Q) and rainfall (RF) time series. **b)** PSD of the East channel. **c)** PSD of the North channel. **d)** PSD of the Vertical channel. **e)** Temporal evolution of the 33-Hz band amplification. **f)** Cross-correlation results between the discharge and the rainfall (Q-RF), and between the selected 33-Hz band and the discharge (PSD-Q).

Snowmelt event: spring 2021

The snowmelt period began after three consecutive days with hourly air temperature persistently above 0 °C (22–25 March), reflecting the seasonal spring warming trend. It produced a gradual increase in discharge, culminating in a smooth peak of 0.350 $m^3 s^{-1}$ (Figure 3a). The discharge record also shows a clear thermally driven diurnal cycle, with daily maxima lagging air temperature by approximately 9 hours (ρ_{xy}= 0.75, Figure 3f and Table 1), consistent with meltwater production and delayed transfer through percolation within the aquifer vadose zone. Relative to extreme rainfall events, this regime is characterized by weaker hydrodynamic forcing, allowing thermal effects to emerge more clearly within the seismic record. Under these conditions, amplification of the 33-Hz band is detectable on all the three components (Figure 3b,c,d), but it is lower than during extreme rainfall, with maxima of approximately −150 dB on the horizontal components (HHN, HHE) and −155 dB on the vertical component (Figure 3e). Unlike the October 2020 flood, no broadband amplification is observed, and the secondary 12-Hz band is only weakly distinguishable. The 33-Hz amplification is essentially in phase with the discharge (ρ_{xy} = 0.98, Figure 3f and Table 1), indicating that snowmelt inflow is distributed over a prolonged period, piston-flow effects are limited, and the discharge increase is mainly sustained by progressive drainage through the system. Consequently, the associated mechanical perturbation is weaker and occurs contemporaneously with

DOI: 10.59490/6ad293c76ee698573e4dd1a1

discharge rather than preceding it, which also facilitates the identification of additional 12-hour thermally modulated cycles in the PSD records.

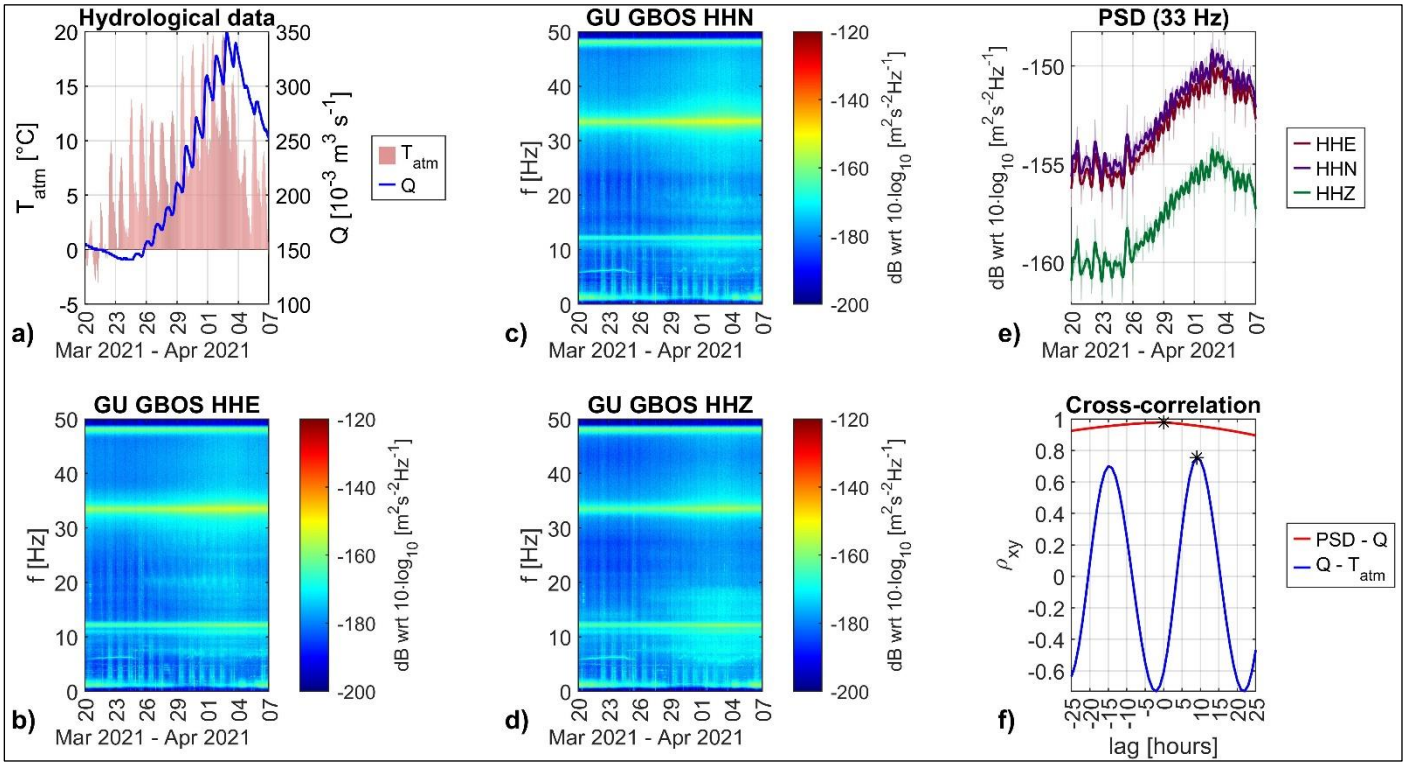


Figure 3. Power spectral densities (PSD) of seismic recordings from 20 March to 7 April 2021, including a seasonal snowmelt event. **a)** Discharge (Q) and atmospheric temperature (T_{atm}) time series. **b)** PSD of the East channel. **c)** PSD of the North channel. **d)** PSD of the Vertical channel. **e)** Temporal evolution of the 33-Hz band amplification. **f)** Cross-correlation results between the discharge and the atmospheric temperature (Q- T_{atm}), and between the selected 33-Hz band and the discharge (PSD-Q).

Rainfall event: spring 2022

The third event enables a direct comparison between the internal (GBOS) and external (S1) seismic signatures. Following the rainfall events, discharge peaks occurred with an approximately 10-hour delay, indicating an intense but not exceptional spring event, with a maximum discharge of 0.681 $m^3 s^{-1}$ (Figure 4g). At station GBOS, the horizontal components (HHE, HHN, Figure 4a and Figure 4b, respectively) show a clear spectral amplification near 33 Hz (maximum amplitude −143 dB, Figure 4h), whereas the vertical component (Figure 4c) is weaker (−148 dB, Figure 4h). The 33-Hz band is essentially synchronous with discharge (zero lag; ρ_{xy} = 0.97, Figure 4i and Table 1), indicating that the seismic response closely follows the hydrodynamic evolution of *Mora* Creek under ordinary rainfall conditions. In contrast, the external station S1 is dominated by an amplified band centred near 30 Hz on the East, North, and Vertical channels (Figure 4d,e,f,). This shift likely reflects different stress-transfer conditions: S1 is buried shallowly (a few tens of centimetres) in soil, whereas GBOS is installed at the meta-carbonate contact within the access conduit. Transient broadband increases in S1 between 35 and 50 Hz occur as localized peaks and are attributed to rainfall-related seismic signatures, consistent with previous research (Dabove et al., 2023). Cross-correlation between the S1 amplified band and discharge shows that the seismic signal leads discharge by 4 hours (lag = −4 h, ρ_{xy} = 0.89, Figure 4i and Table 1): the shallow external sensor may register earlier mechanical perturbations associated with rapid infiltration, though with attenuated amplitudes due to its external location (maxima of -165 dB on the East, -161 dB on the North, and -172 dB on the vertical component, Figure 4h). Conversely, the internal sensor is more directly driven by conduit pressure/discharge dynamics and peaks simultaneously with the main drain discharge; this co-occurrence may mask any earlier stress transients linked to inflowing water. Finally, at both stations, more clearly at S1 and only weakly at GBOS, the moderate magnitude of the rainfall event allows the limited recognition of the additional 12-hour thermally induced cycles in the seismic records.

DOI: 10.59490/6ad293c76ee698573e4dd1a1

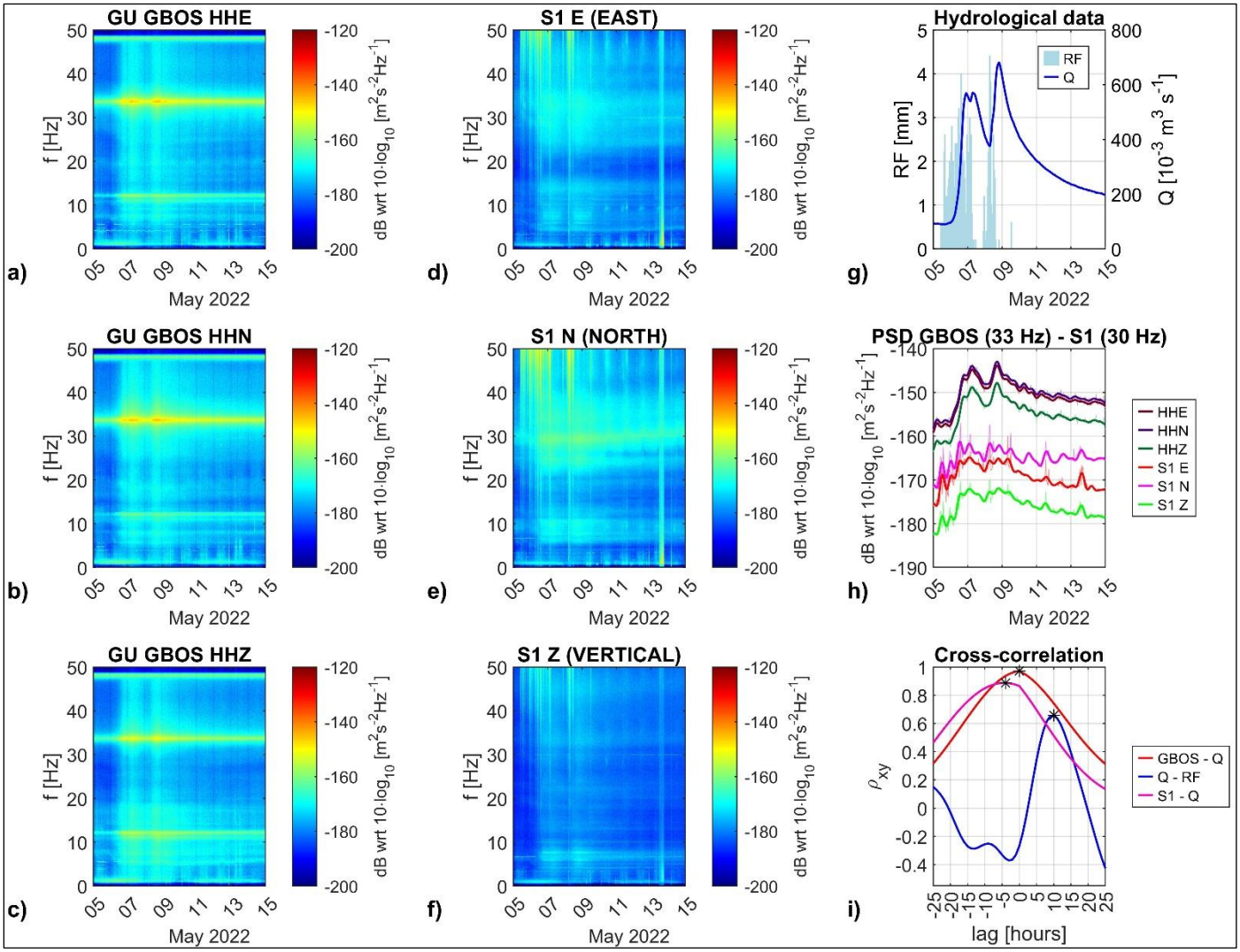


Figure 4. Power spectral densities (PSD) of seismic recordings from 5 to 15 May 2022, acquired at the internal (GBOS) and external (S1) stations. **a)** PSD of the GBOS East channel. **b)** PSD of the GBOS North channel. **c)** PSD of the GBOS Vertical channel. **d)** PSD of the S1 East channel. **e)** PSD of the S1 North channel. **f)** PSD of the S1 Vertical channel. **g)** Discharge (Q) and rainfall (RF) time series. **h)** Temporal evolution of the 33-Hz (GBOS) and 30-Hz (S1) band amplifications. **i)** Cross-correlation results between the discharge and the rainfall (Q- RF), between the selected GBOS 33-Hz band and the discharge (PSD-Q), and between the selected S1 30-Hz band and the discharge (S1-Q).

CONCLUSION

Continuous passive seismic monitoring at the *Bossea* Cave has shown that ambient-noise PSD contains repeatable, hydrologically modulated spectral features that track hydro-mechanical forcing within the karst aquifer. A persistent amplification near 33 Hz at the internal station (GBOS) was strongly correlated with *Mora* Creek discharge and, under ordinary recharge (snowmelt and typical spring rainfall), exhibited an essentially zero-lag response ($\rho_{xy} \approx 0.97$-0.98). During the extreme rainfall–flood event (2–3 October 2020), the PSD increase at 33 Hz preceded peak discharge by 4 hours ($\rho_{xy} = 0.96$), whereas discharge lagged rainfall. This supports a scenario in which rapid infiltration and piston-flow dynamics generate a mechanical stress perturbation that propagates faster than the hydraulic signal controlling the outlet peak. In contrast, snowmelt-driven recharge produced lower-amplitude spectral amplification: discharge was modulated by temperature, with daily maxima lagging air temperature by 9 hours ($\rho_{xy} = 0.75$). This pattern is consistent with delayed transfer through the vadose zone and allows clearer recognition of thermally driven periodicities in the PSD. The internal-external comparison (May 2022) further indicates that spectral responses are also medium-dependent: GBOS was dominated by the 33-Hz band and remained synchronous with discharge, whereas the shallow external station (S1)

DOI: 10.59490/6ad293c76ee698573e4dd1a1

showed a dominant amplified band near 30 Hz and a 4 hour-lead relative to discharge (ρ_{xy} = 0.89). This suggests earlier sensitivity of S1 to near-surface, infiltration-related stress perturbations. Overall, these findings support PSD-based passive seismic monitoring as a complementary tool to hydrometric observations to discriminate impulsive, high-magnitude recharge from gradual seasonal inputs and to constrain the timing of hydro-mechanical loading in fractured karst systems. This integrated evidence also provides a basis for investigating coupled thermo- and hydro-driven rock-mass deformation and for characterizing the spectral signatures of impulsive microseismic signals potentially associated with incipient fracturing.

ACKNOWLEDGEMENTS

The Authors declare no competing interests. During the preparation of this work the Authors used ChatGPT-5.2 in order to improve language and grammar. After using this tool, the Authors reviewed and edited the content as needed and take full responsibility for the content of the published article. The Authors are grateful to Dr. Fabrizio Bosco (*Department of Natural and Environmental Risks, Environmental Protection Agency of Piedmont – ARPA Piemonte*) for supporting GBOS data retrieval from the European Integrated Data Archive (EIDA).

CONTRIBUTION STATEMENT

Conceptualization: L.B., F.V., and C.C.; Data Curation: L.B. and B.V.; Analysis: L.B. and C.C.; Investigation: all the Authors; Methodology: L.B. and C.C.; Visualization: L.B.; Writing: L.B.; Funding acquisition: F.V., A.F., and B.V.; Project administration: B.V.; Supervision: F.V., C.C., and B.V.; Writing - Review & Editing: all the Authors.

REFERENCES

Almagro Vidal, C., Zaccarelli, L., Pintori, F., Bragato, P. L., & Serpelloni, E. (2021). Hydrological effects on seismic-noise monitoring in karstic media. *Geophysical Research Letters*, *48*(15), Article e2021GL093191. https://doi.org/10.1029/2021GL093191

Antonellini, M., Nannoni, A., Vigna, B., & De Waele, J. (2019). Structural control on karst water circulation and speleogenesis in a lithological contact zone: The Bossea cave system (Western Alps, Italy). *Geomorphology*, *345*, Article 106832. https://doi.org/10.1016/j.geomorph.2019.07.019

Bendat, J. S., & Piersol, A. G. (2010). *Random data: Analysis and measurement procedures* (4th ed.). Wiley. https://doi.org/10.1002/9781118032428

Biamino, L., Colombero, C., Fiorucci, A., Peano, G., & Vigna, B. (2024). Natural radon levels act as markers of hydrodynamic behavior in the mountain karst aquifer of Bossea Cave, Italy. *Scientific Reports*, *14*(1), Article 29178. https://doi.org/10.1038/s41598-024-80607-8

Bozzoli, M., Crespi, A., Matiu, M., Majone, B., Giovannini, L., Zardi, D., Brugnara, Y., Bozzo, A., Berro, D. C., Mercalli, L., & Bertoldi, G. (2024). Long-term snowfall trends and variability in the Alps. *International Journal of Climatology*, *44*(13), 4571–4591. https://doi.org/10.1002/joc.8597

Dabove, P., Colombero, C., & Salerno Quaroni, A. (2023). Towards the monitoring of underground caves using geomatics and geophysical techniques: 3D analyses and seismic response. *ISPRS International Journal of Geo-Information*, *12*(5), Article 191. https://doi.org/10.3390/ijgi12050191

Fiorucci, A., Moitre, B., & Vigna, B. (2015). Hydrogeochemical study of Bossea karst system. In *Environmental safety and construction in karst areas* (pp. 290–294). Perm State University.

Fores, B., Champollion, C., Mainsant, G., Albaric, J., & Fort, A. (2018). Monitoring saturation changes with ambient seismic noise and gravimetry in a karst environment. *Vadose Zone Journal*, *17*(1), Article 170163. https://doi.org/10.2136/vzj2017.09.0163

Krischer, L., Megies, T., Barsch, R., Beyreuther, M., Lecocq, T., Caudron, C., & Wassermann, J. (2015). ObsPy: A bridge for seismology into the scientific Python ecosystem. *Computational Science & Discovery*, *8*(1), Article 014003. https://doi.org/10.1088/1749-4699/8/1/014003

McNamara, D. E., & Buland, R. P. (2004). Ambient noise levels in the continental United States. *Bulletin of the Seismological Society of America*, *94*(4), 1517–1527. https://doi.org/10.1785/012003001

DOI: 10.59490/6ad293c76ee698573e4dd1a1

Nannoni, A., Vigna, B., Fiorucci, A., Antonellini, M., & De Waele, J. (2020). Effects of an extreme flood event on an Alpine karst system. *Journal of Hydrology*, *590*, Article 125493. https://doi.org/10.1016/j.jhydrol.2020.125493

Pantiga, A., Allègre, V., Lastennet, R., Houillon, N., Naessens, F., Mateo, S., & Denis, A. (2025). Estimating flow dynamics in a karst conduit from ambient noise monitoring. *Environmental Processes*, *12*(1), Article 11. https://doi.org/10.1007/s40710-025-00752-8

University of Genoa. (1967). *Regional Seismic Network of North Western Italy* [Data set]. International Federation of Digital Seismograph Networks. https://doi.org/10.7914/SN/GU

Vigna, B., & Banzato, C. (2015). The hydrogeology of high-mountain carbonate areas: An example of some Alpine systems in southern Piedmont (Italy). *Environmental Earth Sciences*, *74*(1), 267–280. https://doi.org/10.1007/s12665-015-4308-8

Welch, P. D. (1967). The use of fast Fourier transform for the estimation of power spectra: A method based on time averaging over short, modified periodograms. *IEEE Transactions on Audio and Electroacoustics*, *15*(2), 70–73. https://doi.org/10.1109/TAU.1967.1161901